OPEN

NPG Asia Materials (2017) 9, e361; doi:10.1038/am.2017.26
www.nature.com/am

ORIGINAL ARTICLE

Semimetallic carbon allotrope with a topological nodal line in mixed sp^2-sp^3 bonding networks

Ha-Jun Sung[1], Sunghyun Kim[1], In-Ho Lee[2] and Kee Joo Chang[1]

Graphene is known as a two-dimensional Dirac semimetal, in which electron states are described by the Dirac equation of relativistic quantum mechanics. Three-dimensional analogs of graphene are characterized by Dirac points or lines in momentum space, which are protected by symmetry. Here, we report a novel 3D carbon allotrope belonging to a class of topological nodal line semimetals, discovered using an evolutionary structure search method. The new carbon phase in the monoclinic *C2/m* space group, termed *m*-C_8, consists of five-membered rings with sp^3 bonding interconnected by sp^2-bonded carbon networks. Enthalpy calculations reveal that *m*-C_8 is more favorable than recently reported topological semimetallic carbon allotropes, and the dynamic stability of *m*-C_8 is verified by phonon spectra and molecular dynamics simulations. Simulated X-ray diffraction patterns indicate that *m*-C_8 could be one of the unidentified carbon phases observed in detonation shoot. The analysis of electronic properties indicates that *m*-C_8 exhibits a nodal line protected by both inversion and time-reversal symmetries in the absence of spin-orbit coupling and the surface band connecting the projected nodal points. Our results may help design new carbon allotropes with exotic electronic properties.

NPG Asia Materials (2017) **9,** e361; doi:10.1038/am.2017.26; published online 17 March 2017

INTRODUCTION

Carbon, which is one of the most abundant elements in nature, has a rich variety of structural allotropes due to its capacity to form *sp*, sp^2 and sp^3 hybridized bonds. Graphene, a single layer of carbon in a honeycomb lattice, consists of all-sp^2 bonds and exhibits a semimetallic band structure with Dirac points. Recently, topological materials, including topological insulators (TIs) and topological semimetals (TSMs), have received a great deal of attention because of the intriguing physical phenomena underlying their behavior, as well as their potential applications. The prediction of the TI phase in graphene with spin-orbit coupling (SOC)[1] has stimulated a tremendous amount of theoretical and experimental work to explore new topological materials. The TI state has been demonstrated for two-dimensional (2D) HgTe/CdTe quantum wells[2] and three-dimensional (3D) Bi-based chalcogenides.[3] The band structure of a TI is characterized by the existence of a bulk band gap, as well as gapless boundary states that are protected by the nontrivial topology of bulk electronic states. By contrast, in TSMs, the valence and conduction bands cross each other at discrete points (Dirac and Weyl semimetals) or along curves (nodal line semimetals) in momentum space. In Dirac semimetals, which have been realized with Na_3Bi (ref. 4) and Cd_3As_2,[5] the band crossing points at the Fermi energy have four-fold degeneracy. By breaking either inversion or time-reversal symmetry in Dirac semimetals, one can obtain Weyl semimetals in which each Dirac point splits into a pair of doubly degenerate Weyl points with opposite chirality. Weyl semimetals have been proposed for compounds containing heavy elements, such as pyrochlore iridates,[6] $HgCr_2Se_4$,[7] and transition metal dichalcogenides,[8] and the prediction of the Weyl semimetal state in the TaAs family[9] has been verified experimentally.[10]

In nodal line semimetals, the formation of Dirac nodes along a closed loop or line requires inversion and time-reversal symmetries without SOC in Cu_3(Pd, Zn)N (ref. 11), Ca_3P_2,[12] and alkaline-earth metals (Ca, Sr, Yb)[13] and compounds AX_2 (A = Ca, Sr, Ba; X = Si, Ge, Sn).[14] When SOC is included, additional non-symmorphic symmetry is necessary to protect the nodal line against gap opening in ZrSiS.[15] In non-centrosymmetric $PbTaSe_2$, the nodal line is protected by mirror reflection symmetry even in the presence of SOC.[16] Meanwhile, the TSM phase has also been reported for 3D carbon networks constructed from graphene, such as Mackay-Terrenes crystals,[17] interpenetrated graphene networks (IGNs)[18] and bco-C_{16}.[19] Due to the negligible SOC,[20] the nodal lines of these semimetallic carbon allotropes are protected by a combination of inversion and time-reversal symmetry. Recent experiments have demonstrated the synthesis of 3D graphene networks with high-electrical conductivities by a chemical vapor deposition technique, although the associated crystal structure has not yet been identified.[21] Other 3D metallic carbon allotropes have been proposed, including *H*18 carbon[22] and *T*6 carbon[23] in mixed sp^2-sp^3 bonding networks, and $ThSi_2$-type tetragonal bct4 carbon[24] and *H*6 carbon[25] with all-sp^2 bonding. However, the band overlap occurs at different crystal momenta in *H*18 and *T*6 carbon,[22,23] whereas the metallic nature of bct4 and *H*6 carbon arises from the twisted π states that make these allotropes dynamically unstable.[26]

[1]Department of Physics, Korea Advanced Institute of Science and Technology (KAIST), Daejeon, Korea and [2]Center for Materials Genome, Korea Research Institute of Standards and Science, Daejeon, Korea
Correspondence: Professor KJ Chang, Department of Physics, KAIST, 291 Daehak-ro, Yuseong-gu, Daejeon 34141, Korea.
E-mail: kjchang@kaist.ac.kr
Received 4 November 2016; revised 28 December 2016; accepted 6 January 2017

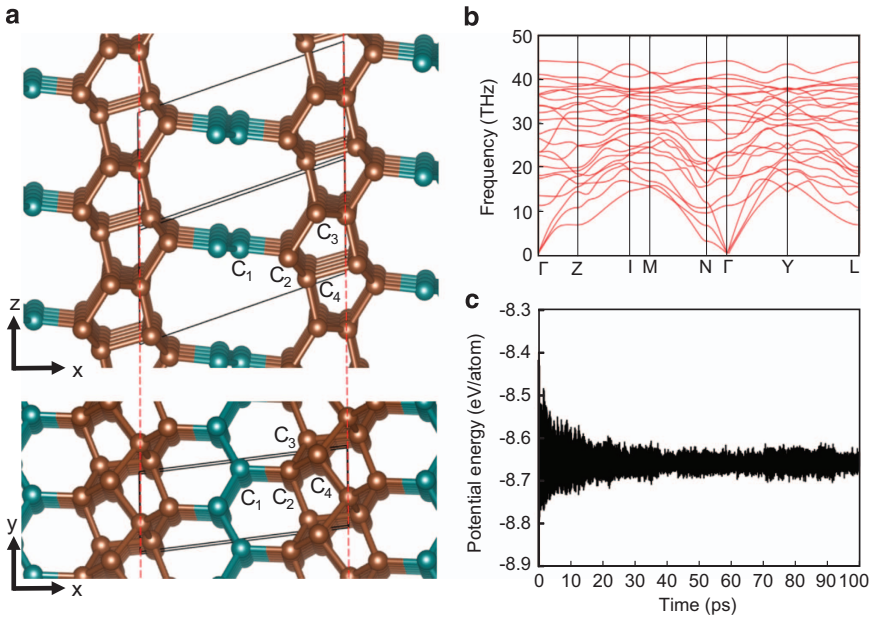

Figure 1 (**a**) Side and top views of the atomic structure of *m*-C_8 in *C2/m* space group. The lattice parameters in the monoclinic structure are $a=7.010$ Å, $b=2.480$ Å, $c=6.608$ Å, $\beta=71.2°$ and C_1, C_2, C_3 and C_4 denote the four inequivalent Wyckoff positions. (**b**) Calculated phonon spectra of *m*-C_8 at zero pressure and (**c**) potential energy fluctuations during MD simulations at 1500 K for a $2\times4\times2$ supercell.

Table 1 Calculated structural and electronic properties of various carbon allotropes

	Method	V_0	*a*	*b*	*c*	$d_{C\text{-}C}$	E_{tot}	E_g
Diamond	AM05	5.60	3.554			1.538	−9.467	5.36
	Exp. ref. 35	5.67	3.567			1.544		5.47
Graphite	AM05	8.79	2.461		6.706	1.421	−9.494	0
	Exp. ref. 36	8.78	2.460		6.704	1.420		0
*T*6	AM05	6.76	2.600		6.000	1.340, 1.540	−8.962	0
IGN	AM05	7.53	2.456		4.291	1.403, 1.519	−9.302	0
bco-C_{16}	AM05	7.71	7.806	4.875	3.239	1.383–1.458	−9.120	0
oC8	AM05	6.48	7.788	2.499	2.665	1.347–1.632	−9.115	0
m-C_8	AM05	6.80	7.010	2.480	6.608	1.412–1.538	−9.251	0

Calculated equilibrium volumes (V_0 in Å^3/atom), lattice parameters (*a*, *b* and *c* in Å), bond lengths ($d_{C\text{-}C}$ in Å), total energies (E_{tot} in eV/atom), and band gaps (E_g in eV) for diamond, graphite, *T*6 carbon, IGN, bco-C_{16}, oC8 and *m*-C_8.

In this work, we report a new 3D carbon allotrope belonging to a class of topological nodal line semimetals, based on global optimization and first-principles density functional calculations. The new carbon phase, termed *m*-C_8, consists of five-membered rings with sp^3 hybridized bonds and sp^2-bonded carbon networks, and the enthalpy of *m*-C_8 is lower than those of recently proposed carbon allotropes with topological nodal lines. The dynamic stability of *m*-C_8 is verified by phonon spectra and molecular dynamics simulations. On the basis of the analysis of X-ray diffraction patterns and enthalpy-pressure curves, we propose that *m*-C_8 may be present in detonation soot[27] and a phase transition from graphite to *m*-C_8 can occur under pressure.

METHODS

Computational structure search and electronic structure calculations

We explored new carbon allotropes with sp^2-sp^3 hybridized bonds by using a computational search method,[28] in which the conformational space annealing (CSA) algorithm[29] for global optimization is combined with first-principles electronic structure calculations. The efficiency of this approach has been demonstrated by successful applications to predict Si and C allotropes with direct band gaps.[30,31] For various carbon systems with *N* atoms per unit cell ($N=8$, 12, 16, 20), we optimized the degrees of freedom, such as atomic positions and lattice parameters, with the number of configurations set to 40 in the population size of the CSA.

The goal of computational materials design is to obtain the optimal crystal structure with specific target properties, which can be expressed in terms of an objective function.[28] In this work, the objective function is composed of two parts: enthalpy and penalty. For all configurations, a local minimization was performed for the enthalpy within the framework of density functional theory. Our work aimed to find low-energy 3D carbon allotropes with exotic electronic properties. Thus, the penalty function was designed to prevent carbon structures from forming all-sp^2 or all-sp^3 hybridized bonds, such as diamond and graphite, and to promote mixed sp^2-sp^3 bonding networks. In each configuration, sp^2- and sp^3-hybridized atoms were determined by using the bond lengths of 1.42 and 1.54 Å. If configurations only consisted of sp^2- or sp^3-hybridized atoms, the penalty function, defined as $f_p(N) = 2\times N$ eV, was included in the objective function, so that configurations with high-objective function values were excluded. For the first-principles calculations we used the

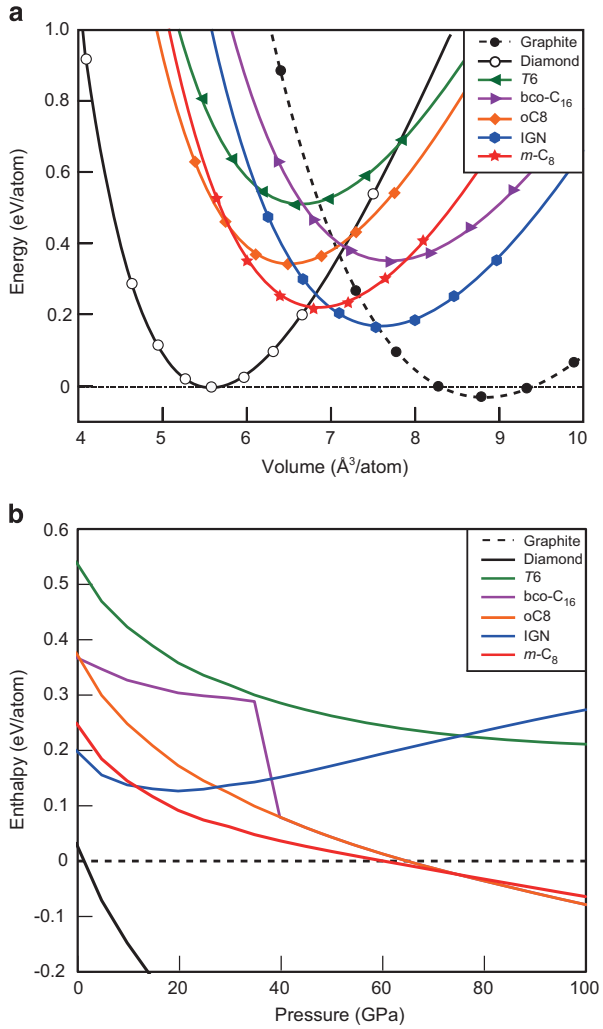

Figure 2 (**a**) Total energy as a function of volume and (**b**) enthalpy as a function of pressure curves for diamond, graphite, *T*6 carbon, IGN, bco-C_{16}, oC8 and *m*-C_8. The transition from graphite to *m*-C_8 occurs at a pressure of 60 GPa.

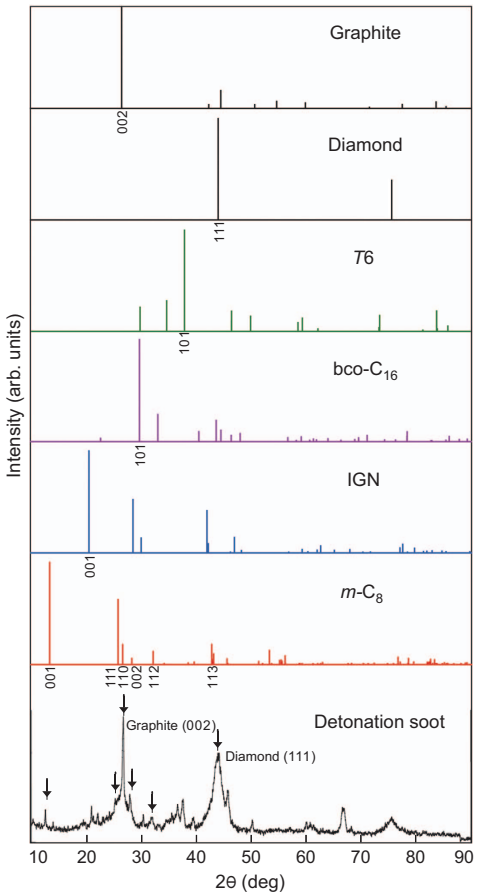

Figure 3 The simulated X-ray diffraction patterns for graphite, diamond, *T*6 carbon, bco-C_{16}, IGN and *m*-C_8 are compared to those experimentally observed for detonation soot of TNT (sample Alaska B).[27] Arrows indicate the X-ray diffraction peaks related to *m*-C_8.

functional form proposed by Armiento and Mattsson (AM05) (ref. 32) for the exchange-correlation potential and the projector augmented wave potentials,[33] as implemented in the VASP code.[34] In graphite, interlayer interactions are described more accurately with the AM05 functional compared to other functional forms of the exchange-correlation potential (Supplementary Table S1). The wave functions were expanded in plane waves up to an energy cutoff of 600 eV. At the final stage of optimization, we used an even higher energy cutoff of 800 eV.

RESULTS AND DISCUSSION

Structure and stability of a new carbon allotrope

Among many low-energy allotropes (Supplementary Table S2), we obtained a very distinctive crystal structure in the *C*2/*m* space group (Figure 1a), especially for the $N=8$ system. For the $N=16$ system, the same low-energy allotrope was also found by the computational search method, although both the number of atoms per unit cell and the cell volume are doubled. The monoclinic *C*2/*m* structure, denoted as *m*-C_8, has the equilibrium lattice parameters, $a=7.010$ Å, $b=2.480$ Å, $c=6.608$ Å and $\beta=71.2°$, and four inequivalent Wyckoff positions, *4i* (0.272, 0, 0.446), (0.632, 0, 0.79), (0.781, 0, −0.072) and (0.007, 0, 0.878), occupied by the C_1, C_2, C_3 and C_4 atoms, respectively. The *m*-C_8 allotrope is characterized by five-membered carbon rings interconnected by graphitic carbon networks, similar to penta-graphene ribbons linked with hexa-graphene ribbons.[37] The graphitic networks are composed of sp^2-bonded C_1 atoms, with the bond length of $d_{C_1-C_1}=1.412$ Å, whereas the C_2, C_3, and C_4 atoms forming five-membered rings are all sp^3-bonded, with the bond lengths of $d_{C_2-C_3}=1.553$ Å, $d_{C_2-C_4}=1.527$ Å, $d_{C_3-C_3}=1.540$ Å, $d_{C_3-C_4}=1.514$ Å and $d_{C_4-C_4}=1.570$ Å. Note that the bond length between the C_1 and C_2 atoms, which connect graphitic sheets to five-membered rings, is $d_{C_1-C_2}=1.493$ Å, between those of graphite (1.420 Å) and diamond (1.544 Å).

In Table 1, the calculated equilibrium volume, lattice parameters, bond lengths and total energy of *m*-C_8 are compared to those of diamond, graphite and several recently reported metallic allotropes: *T*6 carbon[25] and IGN,[20] in mixed sp^2-sp^3 bonding networks, and oC8 carbon[38] and bco-C_{16},[19] in all-sp^2 bonding networks. The equilibrium volume of *m*-C_8 is 6.80 Å^3 per atom, between those of graphite and diamond. Because of the mixture of sp^2 and sp^3 hybridized bonds, the *m*-C_8 allotrope has four different bond angles of 93.7, 107.3, 114.1 and 121.3°, which deviate from the ideal bond angles of graphite (120°) and diamond (109.5°). Owing to the induced strain, the *m*-C_8 structure has an excess energy of 0.22 eV/atom compared to the diamond phase. By contrast, *m*-C_8 is more stable by 0.13–0.29 eV/atom than *T*6 carbon, oC8 carbon and bco-C_{16}. It is interesting to note that although the total energy of *m*-C_8 at the equilibrium volume is higher

by 0.05 eV/atom than that of IGN, its enthalpy is lower for pressures above 10 GPa (Figures 2a and b). From the enthalpy vs pressure curve, a possible synthesis of m-C_8 is expected under compression of graphite. It has been suggested that graphite may transform to oC8 carbon, which is a denser form of bco-C_{16}, above 65 GPa.[19,38] However, our calculations indicate that m-C_8 is lower in enthalpy than bco-C_{16} up to 77 GPa, and a transition from graphite to m-C_8 is more likely to occur at the lower pressure of 60 GPa.

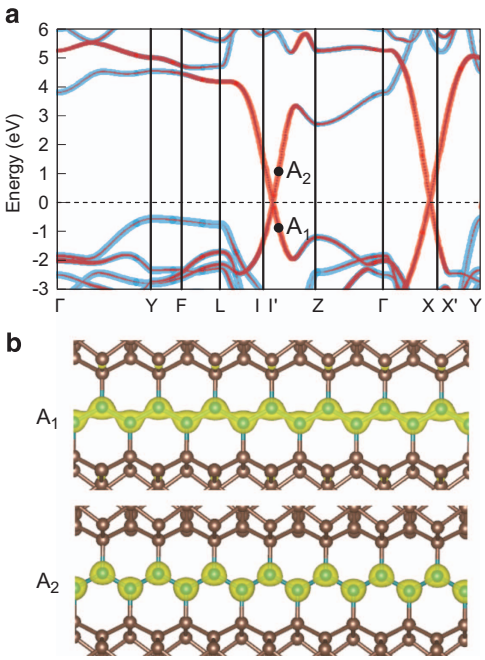

Figure 4 (**a**) Band structure of m-C_8. The thicknesses of the red and blue colored bands represent the degrees of confinement for the sp^2 and sp^3 hybridized atoms, respectively. (**b**) Distribution of the charge densities for the linear bands (A_1 and A_2) near the Fermi energy, which are mainly derived from the carbon chains in the sp^2 bonding networks.

We examined the stability of m-C_8 by calculating the full phonon spectra and found no imaginary phonon modes over the entire Brillouin zone (BZ) (Figure 1b), indicating that m-C_8 is dynamically stable. In addition, we carried out first-principles molecular dynamics (MD) simulations at a temperature of 1500 K. For a $2 \times 4 \times 2$ supercell containing 128 atoms, we confirmed that the m-C_8 allotrope is stable for up to 100 ps (Figure 1c). Owing to the thermal stability, the synthesis of m-C_8 is expected under high-pressure and high-temperature. We also calculated the elastic constants of m-C_8, and confirmed that the elastic constants meet the criteria for mechanical stability in monoclinic structure.[39]

The X-ray diffraction patterns of m-C_8 were simulated and compared to the experimental data from detonation soot (sample Alaska B),[27] along with those of graphite, diamond, *T*6 carbon, bco-C_{16} and IGN, as shown in Figure 3. In the detonation soot, the prominent peaks ~26.5° and 43.9° are attributed to the graphite (002) and diamond (111) diffractions, respectively. The (101) peak of *T*6 carbon, (101) peak of bco-C_{16}, and (001) peak of IGN match with the experimental X-ray diffraction data located at 37.4°, 30.0° and 21.4°, respectively. However, the low-angle peak at 13.4° does not match any previously reported carbon phases. This peak was also observed in different detonation soot,[27] indicating that an unknown carbon phase should be produced. Our simulated X-ray diffraction results show that the main (001) peak of m-C_8 reasonably explains the unidentified peak at 13.4°. Moreover, the (111), (002) and (112) peaks of m-C_8 match those in the experimental X-ray diffraction pattern located at 25.1°, 27.8° and 32.1°, respectively, indicating the presence of m-C_8 in the specimen produced by detonation experiments.[27]

Band structure of a new carbon allotrope

Finally, we examined the band topology of m-C_8. In Figure 4a, the band structure exhibits linear dispersions around the Fermi level where the valence and conduction bands touch, similar to graphene. The linear bands are mainly derived from the sp^2 hybridized C atoms in graphitic sheets, as illustrated in the distribution of charge densities

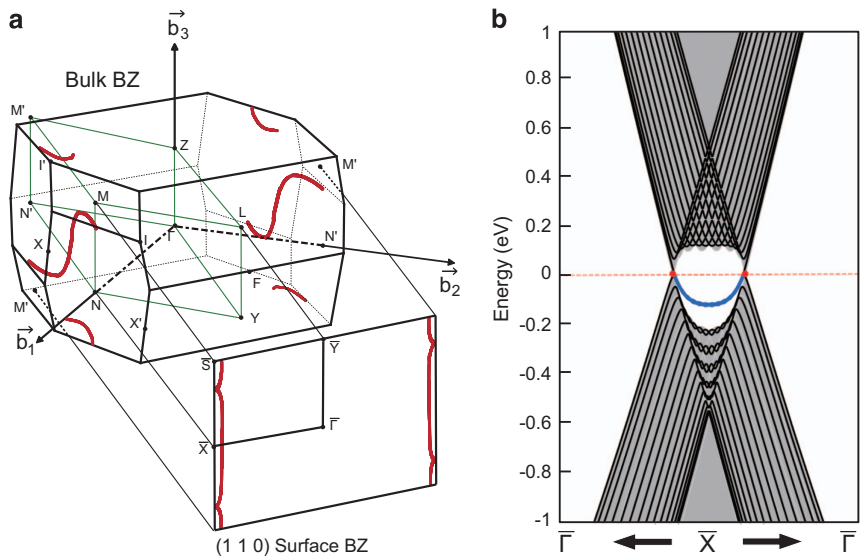

Figure 5 (**a**) The 3D Brillouin zone (black polyhedron) with several high-symmetry momenta and the nodal lines (red lines) at the Fermi energy in the monoclinic structure of m-C_8. TRIM points (vertices in green rhombohedral) and their projection onto the (110) surface BZ are indicated. (**b**) Topologically protected (110)-surface band (blue line) nestled inside the bulk nodal line (red dots).

Table 2 Parity eigenvalues of *m*-C_8

TRIM	δ	*TRIM*	δ
$\Gamma(\Lambda_{0,0,0})$	+1	$N(\Lambda_{1/2,0,0})$	+1
$Y(\Lambda_{1/2,1/2,0})$	−1	$N'(\Lambda_{0,1/2,0})$	+1
$Z(\Lambda_{0,0,1/2})$	−1	$M(\Lambda_{1/2,0,1/2})$	+1
$L(\Lambda_{1/2,\ 1/2,\ 1/2})$	+1	$M'(\Lambda_{0,1/2,1/2})$	+1

Product of parity eigenvalues (δ) for the occupied bands at the time-reversal invariant momenta (TRIM) in *m*-C_8.

(Figure 4b), whereas more dispersive bands far from the Fermi level are associated with the sp^3 hybridized bonds in five-membered rings. From the band structure in the full BZ, we find that the crossing points of the valence and conduction bands form a continuous nodal line piercing the extended BZ, without interfering with sp^3-hybridized bands (Figures 4 and 5). Thus, the *m*-C_8 allotrope with symmorphic symmetry belongs to a class of topological nodal line semimetals.[11–19] Recently, two types of topological nodal line semimetals were proposed, depending on systems with and without SOC.[39] In the former, because the SOC may open up gaps at the band crossing points, both inversion and time-reversal symmetries are insufficient to protect the band crossings, whereas additional non-symmorphic symmetry can protect the nodal line.[40] In carbon systems such as *m*-C_8, with a negligible SOC, the topological nodal line survives by a combination of inversion and time-reversal symmetries.

Based on the analysis of parity eigenvalues, Fu and Kane proposed the Z_2 topological invariants $(v_0; v_1v_2v_3)$ to describe the topological nature of TIs.[41] Similarly, the parities of energy states can be used to assign the Z_2 topological invariants in topological nodal line semimetals. For the eight time-reversal invariant momenta (Figure 5a), the products of the parity eigenvalues (δ) for the occupied bands are listed in Table 2. We found that *m*-C_8 is characterized by the weak Z_2 indices (0;111) due to the value of $\delta = -1$ at the Y and Z points. As *m*-C_8 has no mirror reflection symmetry, the bulk nodal line does not appear in a mirror-invariant plane. To visualize the formation of topological surface states, we calculated the surface band structure for a slab geometry composed of 20 graphitic layers, where the (110) surface is exposed to vacuum. As the bulk BZ is projected onto the (110) surface BZ, one can expect that the nodal line is located near the $\overline{X}$ and $\overline{S}$ points (Figure 5a). In fact, the projected band structure clearly shows the formation of the nearly flat surface state connecting the projected nodal points around the $\overline{X}$ point (Figure 5b).

In summary, we have predicted a novel carbon allotrope *m*-C_8 with mixed sp^2-sp^3 bonding networks using the evolutionary structure search method. The monoclinic structure of *m*-C_8 is composed of five-membered rings connected by graphitic sheets. The stability of *m*-C_8 is verified by calculating the full phonon spectra and MD simulations at a temperature of 1500 K. From the analysis of the electronic band structure, we have identified that *m*-C_8 belongs to the class of topological nodal line semimetals, exhibiting the topological nodal line in bulk and the topological surface states at surface boundaries. As the SOC is extremely weak in *m*-C_8, the nodal line is protected by the coexistence of inversion and time-reversal symmetries. Although it remains a challenge to synthesize the crystalline form of *m*-C_8, our results provide not only a perspective for the novel electronic structure of carbon allotropes but also promote future studies to explore new carbon allotropes with exotic electronic and transport properties.

CONFLICT OF INTEREST

The authors declare no conflict of interest.

ACKNOWLEDGEMENTS

This work was supported by Samsung Science and Technology Foundation under Grant No. SSTF-BA1401-08.

1 Kane, C. L. & Mele, E. J. Quantum spin Hall effect in graphene. *Phys. Rev. Lett.* **95**, 226801 (2005).
2 König, M., Wiedmann, S., Brüne, C., Roth, A., Buhmann, H., Molenkamp, W., Qi, X.-L. & Zhang, S.-C. Quantum spin hall insulator state in HgTe quantum wells. *Science* **318**, 766–770 (2007).
3 Xia, Y., Qian, D., Hsieh, D., Wray, L., Pal, A., Lin, H., Bansil, A., Grauer, D., Hor, Y. S., Cava, R. J. & Hasan, M. Z. Observation of a large-gap topological-insulator class with a single Dirac cone on the surface. *Nat. Phys.* **5**, 398–402 (2009).
4 Liu, Z. K., Zhou, B., Zhang, Y., Wang, Z. J., Weng, H. M., Prabhakaran, D., Mo, S.-K., Shen, Z. X., Fang, Z., Dai, X., Hussain, Z. & Chen, Y. L. Discovery of a three-dimensional topological Dirac semimetal, Na_3Bi. *Science* **343**, 864–867 (2014).
5 Neupane, M., Xu, S.-Y., Sankar, R., Alidoust, N., Bian, G., Liu, C., Belopolski, I., Chang, T.-R., Jeng, H.-T., Lin, H., Bandsil, A., Chou, F. & Hasan, M. Z. Observation of a three-dimensional topological Dirac semimetal phase in high-mobility Cd_3As_2. *Nat. Commun.* **5**, 3786 (2014).
6 Wan, X., Turner, A. M., Vishwanath, A. & Savrasov, S. Y. Topological semimetal and Fermi-arc surface states in the electronic structure of pyrochlore iridates. *Phys. Rev. B* **83**, 205101 (2011).
7 Xu, G., Weng, H., Wang, Z., Dai, X. & Fang, Z. Chern semimetal and the quantized anomalous Hall effect in $HgCr_2Se_4$. *Phys. Rev. Lett.* **107**, 186806 (2011).
8 Soluyanov, A. A., Gresch, D., Wang, Z., Wu, Q., Troyer, M., Dai, X. & Bernevig, B. A. Type-II Weyl semimetals. *Nature* **527**, 495–498 (2015).
9 Weng, H., Fang, C., Fang, Z., Bernevig, B. A. & Dai, X. Weyl semimetal phase in noncentrosymmetric transition-metal monophosphides. *Phys. Rev. X* **5**, 011029 (2015).
10 Lv, B. Q., Weng, H. M., Fu, B. B., Wang, X. P., Miao, H., Ma, J., Richard, P., Huang, X. C., Zhao, L. X., Chen, G. F., Fang, Z., Dai, X., Qian, T. & Ding, H. Experimental discovery of weyl semimetal TaAs. *Phys. Rev. X* **5**, 031013 (2015).
11 Kim, Y., Wieder, B. J., Kane, C. L. & Rappe, A. M. Dirac line nodes in inversion-symmetric crystals. *Phys. Rev. Lett.* **115**, 036806 (2015).
12 Xie, L. S., Schoop, L. M., Seibel, E. M., Gibson, Q. D., Xie, W. & Cava, R. J. A new form of Ca_3P_2 with a ring of Dirac nodes. *APL Mater.* **3**, 083602 (2015).
13 Hirayama, M., Okugawa, R., Miyake, T. & Murakami, S. Topological Dirac nodal lines in fcc Calcium, Strontium, and Ytterbium. Preprint at https://arxiv.org/abs/1602.06501 (2016).
14 Huang, H., Liu, J., Vanderbilt, D. & Duan, W. Topological nodal-line semimetals in alkaline-earth stannides, germanides, and silicides. *Phys. Rev. B* **93**, 201114 (2016).
15 Neupane, M., Belopolski, I., Hosen, M. M., Sanchez, D. S., Sankar, R., Szlawska, M., Xu, S.-Y., Dimitri, K., Dhalkal, N., Maldonado, P., Oppeneer, P. M., Kaczorowski, D., Chou, F., Hasan, M. Z. & Durakiewicz, T. Observation of topological nodal fermion semimetal phase in ZrSiS. *Phys. Rev. B* **93**, 201104 (2016).
16 Bian, G., Chang, T.-R., Sankar, R., Xu, S.-Y., Zheng, H., Neupert, T., Chiu, C.-K., Huang, S.-M., Chang, G., Belopolski, I., Sanchez, D.S., Neupane, M., Alidoust, N., Liu, C., Wang, B., Lee, C.-C., Jeng, H.-T., Zhang, C., Yuan, Z., Jia, S., Bansil, A., Chou, F., Lin, H. & Hasan, M.Z. Topological nodal-line fermions in spin-orbit metal $PbTaSe_2$. *Nat. Commun.* **7**, 10556 (2016).
17 Weng, H., Liang, Y., Xu, Q., Yu, R., Fang, Z., Dai, X. & Kawazoe, Y. Topological node-line semimetal in three-dimensional graphene networks. *Phys. Rev. B* **92**, 045108 (2015).
18 Chen, Y., Xie, Y., Yang, S. A., Pan, H., Zhang, F., Cohen, M. L. & Zhang, S. Nanostructured carbon allotropes with Weyl-like loops and points. *Nano Lett.* **15**, 6974–6978 (2015).
19 Wang, J.-T., Weng, H., Nie, S., Fang, Z., Kawazoe, Y. & Chen, C. Body-centered orthorhombic C_{16}: A novel topological node-line semimetal. *Phys. Rev. Lett.* **116**, 195501 (2016).
20 Yao, Y., Ye, F., Qi, X.-L., Zhang, S.-C. & Fang, Z. Spin-orbit gap of graphene: first-principles calculations. *Phys. Rev. B* **75**, 041401 (2007).
21 Chen, Z., Ren, W., Gao, L., Liu, B., Pei, S. & Cheng, H.-M. Three-dimensional flexible and conductive interconnected graphene networks grown by chemical vapour deposition. *Nat. Mater.* **10**, 424–428 (2011).
22 Zhao, C.-X., Niu, C.-Y., Qin, Z.-J., Ren, X. Y., Wang, J.-T., Cho, J.-H. & Jia, Y. H_{18} Carbon: a new metallic phase with sp^2-sp^3 hybridized bonding network. *Sci. Rep.* **6**, 21879 (2016).
23 Zhang, S., Wang, Q., Chen, X. & Jena, P. Stable three-dimensional metallic carbon with interlocking hexagons. *Proc. Natl. Acad. Sci. USA* **110**, 18809–18813 (2013).
24 Hoffmann, R., Hughbanks, T., Kertész, M. & Bird, P. H. A hypothetical metallic allotrope of carbon. *J. Am. Chem. Soc.* **105**, 4831–4832 (1983).
25 Liu, A. Y., Cohen, M. L., Hass, K. C. & Tamor, M. A. Structural properties of a three-dimensional all-sp^2 phase of carbon. *Phys. Rev. B* **43**, 6742 (1991).
26 Wang, J.-T., Chen, C. & Kawazoe, Y. New carbon allotropes with helical chains of complementary chirality connected by Ethene-type π-conjugation. *Sci. Rep* **3**, 3077 (2013).

27 Pantea, D., Brochu, S., Thiboutot, S., Ampleman, G. & Scholz, G. A morphological investigation of soot produced by the detonation of munitions. *Chemosphere* **65**, 821–831 (2006).
28 Lee, I.-H., Oh, Y. J., Kim, S., Lee, J. & Chang, K. J. *Ab initio* materials design using conformational space annealing and its application to searching for direct band gap silicon crystals. *Comp. Phys. Commun.* **203**, 110–121 (2016).
29 Lee, J., Lee, I.-H. & Lee, J. Unbiased global optimization of Lennard-Jones clusters for $N \leq 201$ using the conformational space annealing method. *Phys. Rev. Lett.* **91**, 080201 (2003).
30 Lee, I.-H., Lee, J., Oh, Y. J., Kim, S. & Chang, K. J. Computational search for direct band gap silicon crystals. *Phys. Rev. B* **90**, 115209 (2014).
31 Oh, Y. J., Lee, I.-H., Kim, S., Lee, J. & Chang, K. J. Direct band gap carbon superlattices with efficient optical transition. *Phys. Rev. B* **93**, 085201 (2016).
32 Armiento, R. & Mattsson, A. E. Functional designed to include surface effects in self-consistent density functional theory. *Phys. Rev. B* **72**, 085108 (2005).
33 Blöchl, P. E. Projector augmented-wave method. *Phys. Rev. B* **50**, 17953 (1994).
34 Kresse, G. & Furthmüller, J. Efficient iterative schemes for *ab initio* total-energy calculations using a plane-wave basis set. *Phys. Rev. B* **54**, 11169 (1996).
35 Occelli, F., Loubeyre, P. & Letoullec, R. Properties of diamond under hydrostatic pressures up to 140 GPa. *Nat. Mater.* **2**, 151–154 (2003).
36 Hanfland, M., Beister, H. & Syassen, K. Graphite under pressure: Equation of state and first-order Raman modes. *Phys. Rev. B* **39**, 12598 (1989).
37 Zhang, S., Zhou, J., Wang, Q., Chen, X., Kawazoe, Y. & Jena, P. Penta-graphene: A new carbon allotrope. *Proc. Natl. Acad. Sci. USA* **112**, 2372–2377 (2015).
38 Wang, J.-T., Chen, C. & Kawazoe, Y. Phase conversion from graphite toward a simple monoclinic sp^3-carbon allotrope. *J. Chem. Phys.* **137**, 024502 (2012).
39 Wu, Z.-J., Zhao, E.-J., Xiang, H.-P., Hao, X.-F., Liu, X.-J. & Meng, J. Crystal structures and elastic properties of superhard IrN_2 and IrN_3 from first principles. *Phys. Rev. B* **76**, 054115 (2007).
40 Fang, C., Chen, Y., Kee, H.-Y. & Fu, L. Topological nodal line semimetals with and without spin-orbital coupling. *Phys. Rev. B* **92**, 081201 (2015).
41 Fu, L. & Kane, C. L. Topological insulators with inversion symmetry. *Phys. Rev. B* **76**, 045302 (2007).

Supplementary Information accompanies the paper on the NPG Asia Materials website (http://www.nature.com/am)